Multiturn simulation of radiative Bhabha scattering in the equivalent photon approximation

Peter Kicsiny,[1,2,*] Xavier Buffat,[1] Daniel Schulte,[1] Helmut Burkhardt,[1] Tatiana Pieloni,[2] and Mike Seidel[2]

[1]*European Organisation for Nuclear Research (CERN), CH 1211 Geneva 23, Switzerland*
[2]*École Polytechnique Fédérale de Lausanne (EPFL), Route Cantonale, 1015 Lausanne, Switzerland*

(Received 22 May 2024; accepted 8 August 2024; published 27 September 2024)

In this paper, we present a Monte Carlo event generator for radiative Bhabha scattering, based on the method of equivalent photons, and optimized for multiturn tracking simulations in the XSUITE framework. We demonstrate the accuracy of the event generator with successful benchmarks of the luminosity and event cross section against currently existing alternative tools. Consequently, we use it to investigate existing estimates of the radiative Bhabha scattering beam lifetime at the FCC-ee, as well as the impact of radiative Bhabha scattering on the beam dynamics, using full nonlinear tracking models.

DOI: 10.1103/PhysRevAccelBeams.27.091001

I. INTRODUCTION

The Future Circular Collider (FCC) [1] is a proposed high energy particle collider of about 90 km circumference [2]. Its first stage, the FCC-ee, is aimed to collide electrons and positrons at unprecedented luminosities in order to refine the statistical precision of properties of Standard Model particles.

The power loss due to synchrotron radiation is one of the main challenges in the FCC-ee machine design. Apart from radiation in the bending arcs, the particles can also emit photons during beam-beam collisions, as a result of bending in the collective electromagnetic (EM) field of the opposite bunches, called beamstrahlung [3]. In addition, they can scatter in the field of an individual particle from the opposite beam, an effect called Bhabha scattering in the ultrarelativistic regime [4].

The deflection of the primaries can lead to radiation with photon energies up to the beam energy, an effect called radiative Bhabha scattering, illustrated in Fig. 1. The dynamics of radiative Bhabha scattering is very similar to that of bremsstrahlung in ordinary matter [5,6]. Counting the primaries scattered with a very small angle, which is dominated by the t-channel scattering process both for the elastic ($e^+e^- \to e^+e^-$) and radiative ($e^+e^- \to e^+e^-\gamma$) Bhabha scattering processes, provides a way to measure luminosity in the collider with high precision, which has already been exploited in previous colliders, such as LEP [7]. This small angle Bhabha scattering is one of the processes considered for luminosity measurement at the FCC-ee as well [1].

Although the number of emitted Bhabha photons is much smaller compared to those emitted due to beamstrahlung or synchrotron radiation, due to their relatively high energy, the effect still impacts the beam lifetime. Until now, the estimates for the FCC-ee lifetime contribution from this process are obtained with rough analytical calculations [1,8,9], but no simulations have been performed so far to verify or fine-tune these. Furthermore, although suspected, it is not yet demonstrated with simulations that the energy loss does not result in the change of beam dynamics, e.g., in the form of emittance growth. These points provide a strong motivation to study radiative Bhabha scattering in the frame of the FCC-ee design.

In this paper, we discuss the implementation of a Monte Carlo event generator to simulate photon emission from the radiative Bhabha scattering, optimized for multiturn tracking simulations in the XSUITE framework [10]. We use this event generator to study the FCC-ee beam lifetime and the impact of radiation on beam dynamics. This paper is organized as follows: Sec. II introduces the theory of modeling radiative Bhabha scattering with the method of equivalent photons. Section III details the implementation of the event generator in XSUITE. Section IV presents a benchmark of the radiative Bhabha scattering lifetime obtained by simulating a single beam-beam collision with XSUITE, against BBBREM, with further comparisons of the luminosity per bunch crossing between XSUITE and GUINEA-PIG and that of the cross section between the three codes. Section V presents lifetime estimates obtained from multiturn tracking with XSUITE, using a linear transfer map,

*Contact author: peter.kicsiny@cern.ch

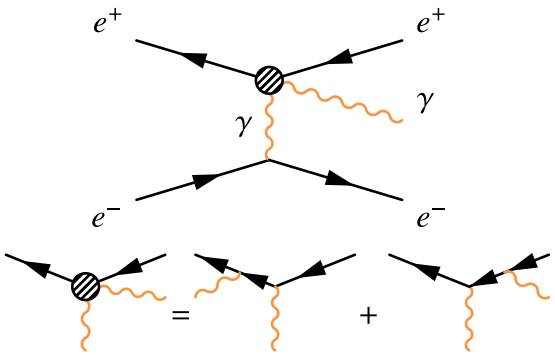

FIG. 1. Top: Main Feynman diagram of radiative Bhabha scattering at small scattering angles, with the exchange of a virtual photon and the emission of a real photon. The symbol γ indicates a photon, and $e^{\pm}$ indicate a positron or an electron, respectively. Bottom: the upper part of the Feynman diagram can be understood as the Compton scattering of the virtual photon on the opposing primary. The blob indicates that this process is described by two Feynman diagrams, each of which is a first order radiative correction to Bhabha scattering.

including effective synchrotron radiation, beamstrahlung, and the crab-waist scheme [11]. Section VI discusses lifetimes and beam dynamics when using a full nonlinear lattice model of the FCC-ee.

II. MODELING OF RADIATIVE BHABHA SCATTERING IN THE EQUIVALENT PHOTON APPROXIMATION

The goal of the work presented in this paper is to model radiative Bhabha scattering in multiturn tracking simulations. In this case, the exact quantum electrodynamical (QED) computation of the scattering process is numerically expensive and impractical. Early works of Fermi have shown that the EM field surrounding a fast moving charged particle is similar to EM radiation [12]. This radiation field can be represented by a flux of photons with a frequency distribution. In case of the collision of two charged particles, the interaction is mathematically equivalent to the interaction of one of the particles with a spectrum of photons equivalent to the other. In the relativistic case, the EM field of a charged particle is almost transversal to the direction of its motion and can, therefore, accurately be substituted by an appropriately chosen equivalent radiation field of photons. With this, the cross section for radiative Bhabha scattering in the forward region, with small scattering angles, can be approximated by that of the e^- or e^+ and a photon in a regular Compton scattering event. In this case, the equivalent photon corresponds to the exchanged virtual photon between the scattering primaries. The subsequent emission of bremsstrahlung photons can be treated in a numerical simulation as an inverse Compton scattering process [13]. This is called the method of equivalent photons and was extended for ultrarelativistic collisions by Weizsäcker and Williams [14,15]. This approach can be used to model the cross section σ_{Bhabha} of radiative Bhabha scattering in a numerical simulation, assuming small scattering angles, by factorizing it into the distribution of the equivalent (virtual) photons and the classical Compton cross section:

$$d\sigma_{\text{Bhabha}} \approx dn \times d\sigma_C, \tag{1}$$

where dn is the number density of the virtual photons representing the equivalent EM field of one primary, and $d\sigma_C$ is the classical Compton scattering cross section. The equivalent photon approximation essentially alleviates the need for computing the QED matrix element with radiative corrections by instead modeling radiative Bhabha scattering as Compton scattering of a set of virtual photons, equivalent to one primary, on the opposing primary. This approach is analogous to the parton distribution functions employed for quarks and gluons in proton-proton collisions [16].

A. Spectrum of virtual photons

In collisions of ultrarelativistic charges ($v \sim c$), with small scattering angles the momentum transfer between the scattering primaries is small, thus it can be assumed that the virtual photons, which are related to this momentum transfer, have a low energy $E_\gamma \ll E_e$ (soft photons), with E_e denoting the total energy of the primary particle and E_γ that of an equivalent virtual photon. Furthermore, it can be shown that the integration over the final momentum space of a scattered primary can be written as an integration over $dxdQ^2$ [17], where x is the virtual photon energy normalized to that of the equivalent primary particle, defined as

$$x = \frac{\hbar\omega}{E_e} = \frac{E_\gamma}{E_e}, \tag{2}$$

with ω being the virtual photon angular frequency, and Q^2 is the squared virtuality of one virtual photon, which is related to its transverse momentum and the momentum transfer between the scattering primaries. With this, the number density spectrum of the virtual photons dn, introduced in Eq. (1), can be expressed as

$$\frac{dn(x,Q^2)}{dxdQ^2} = \frac{\alpha}{2\pi}\frac{1+(1-x)^2}{x}\frac{1}{Q^2}, \tag{3}$$

with $\alpha = 1/137$. The virtual photon energy spectrum is given by integrating Eq. (3) over the interval $[Q^2_{\text{min}}, Q^2_{\text{max}}]$:

$$\begin{aligned}\frac{dn}{dx} &= \int_{Q^2_{\text{min}}}^{Q^2_{\text{max}}} \frac{dn}{dxdQ^2}\,dQ^2 = \frac{\alpha}{2\pi}\frac{1+(1-x)^2}{x}\ln\left(\frac{Q^2_{\text{max}}}{Q^2_{\text{min}}}\right) \\ &\approx \frac{\alpha}{\pi}\frac{1}{x}\ln\left(\frac{Q^2_{\text{max}}}{Q^2_{\text{min}}}\right) = \frac{2\alpha}{\pi}\frac{1}{x}\ln\left(\frac{1}{x}\right),\end{aligned} \tag{4}$$

where we used the approximations

$$\frac{1+(1-x)^2}{x} \approx \frac{2}{x}, \tag{5}$$

$$Q^2_{\min} = \frac{x^2 m_e^2 c^2}{1-x} \approx x^2 m_e^2 c^2, \tag{6}$$

and

$$Q^2_{\max} \approx m_e^2 c^2, \tag{7}$$

by assuming that the virtual photon energy is small ($x \ll 1$) compared to the energy of the scattering primaries. The expression for $Q^2_{\min}$ comes from the kinematically allowed minimum momentum transfer between the scattering primaries. The expression for $Q^2_{\max}$ is typically selected differently, depending on the actual physical process [18]. In case of radiative Bhabha scattering, it is possible to choose it as the dynamic cutoff of the Compton cross section [17,19].

We can make these assumptions in case of small angle Bhabha scattering; however, later when we sample the virtual photons, we need to correct for these approximations. In order to sample photons from Eq. (4), the distribution has to be normalized over the relevant range of x, such that:

$$\frac{dn(x)}{dx} = n_{\text{tot}} f(x), \tag{8}$$

where $f(x)$ is a probability density function (PDF) and n_{tot} is a normalization factor, which represents the total number of virtual photons equivalent to a single primary with total energy E_e. The maximum possible value of x is 1. Since the indefinite integral $\int \frac{1}{x}\ln(\frac{1}{x})dx = -\frac{1}{2}\ln^2(\frac{1}{x}) + C$ diverges into $-\infty$ at 0, an appropriate lower limit $x_{\min}$ on the virtual photon energy has to be set. In practice, the value of this cutoff depends on the physical process, which is being approximated. As we will describe it in Sec. IV, we choose it as the highest value for which the radiative Bhabha cross section is converged, such that virtual photons with a very low energy, which do not contribute to the cross section, are not generated. The normalization factor n_{tot} with a given $x_{\min}$ can be expressed as

$$n_{\text{tot}} = \int_{x_{\min}}^{1} \frac{dn(x)}{dx} dx = \frac{\alpha}{\pi}\ln^2(x_{\min}). \tag{9}$$

Thus the normalized virtual photon density from Eq. (8) can be written as

$$f(x) = \frac{2}{\ln^2(x_{\min})}\frac{1}{x}\ln\left(\frac{1}{x}\right) = C_f \times \frac{1}{x}\ln\left(\frac{1}{x}\right), \tag{10}$$

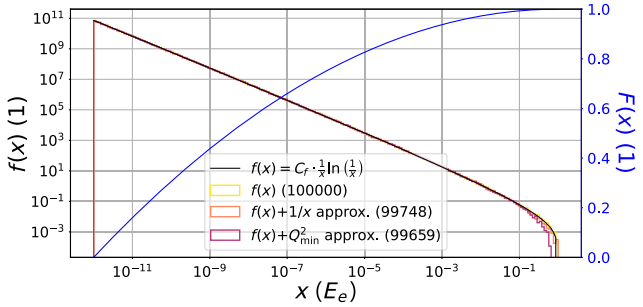

FIG. 2. Normalized virtual photon fluence from Eq. (11) (blue) and flux from Eq. (10) (black) for $E_e = 182.5$ GeV and $x_{\min} = 10^{-12}$. A set of 10^5 events sampled from Eq. (10) are shown. The corrections for the two approximations in Eqs. (5) and (6) are shown with the number of samples surviving the approximation in brackets.

with the constant $C_f = \frac{2}{\ln^2(x_{\min})}$. The corresponding cumulative distribution function (CDF) of Eq. (10) is

$$F(x) = \int_{x_{\min}}^{x} f(x)dx = 1 - \frac{C_f}{2}\ln^2\left(\frac{1}{x}\right) = 1 - C'_f \ln^2(x), \tag{11}$$

with the constant $C'_f = \frac{C_f}{2} = \frac{1}{\ln^2(x_{\min})}$. Eq. (11) can be inverted and used for sampling the original virtual photon distribution in Eq. (4). Figure 2 shows the CDF [Eq. (11)] and PDF [Eq. (10)] of virtual photons for an example energy $E_e = 182.5$ GeV and a low energy cutoff of $x_{\min} = 10^{-12}$. It can be seen that the approximations made in Eqs. (5) and (6) have only a minor effect on the shape of the sampled distribution, in particular at large x values. Since the equivalent photon density depends on the logarithm of the virtuality, Q^2 has to be sampled uniformly in the $[\ln(Q^2_{\min}), \ln(Q^2_{\max})]$ interval.

1. Beam size effect

The beam size effect reduces the number of emitted soft (low energy) photons. The energy spectrum of radiative Bhabha photons, which takes into account the beam size effect corresponds better to experimental measurements, in that roughly a factor of 2 less photons are produced compared to the case without it [5,20]. This in turn reduces the cross section and increases the lifetime by about a factor of 2. The beam size effect in this context is analogous to an effect called screening in classical bremsstrahlung in matter [17]. In the context of beams in particle accelerators, the scattering virtual photon is assumed not to interact with the opposing beam if the impact parameter is more than roughly the transverse rms beam size from the opposite primary.

The beam size effect can be treated in a numerical model by smearing the transverse coordinates of the sampled

virtual photons on a disc of radius ρ, corresponding to the impact parameter (with a random uniform azimuthal angle), thereby giving each photon a different impact parameter, expressed as [21]

$$\rho = \frac{\gamma c}{\omega} = \frac{\hbar c E_e}{m_e c^2 E_\gamma} = \frac{\hbar}{m_e c x} = \frac{\hbar}{\sqrt{Q^2(1-x)}}, \quad (12)$$

where $\gamma = E_e/(m_e c^2)$ is the relativistic Lorentz factor of the primary beam, and x is the normalized virtual photon energy, from Eq. (2). Here, Eq. (6) was used to express the denominator in terms of the virtuality, assuming small scattering angles.

B. Compton scattering of virtual photons

Radiative Bhabha scattering at very small scattering angles can be treated as an inverse Compton scattering process of the virtual photons on the opposite primary. The setup is sketched in Fig. 3.

The total energy E'_γ of the scattered photon from the inverse Compton scattering can be derived from the energy and momentum conservation laws. Using the notations of Fig. 3, these read:

$$\begin{aligned} \gamma m_e c^2 + \hbar\omega &= \gamma' m_e c^2 + \hbar\omega', \\ \gamma m_e v \begin{pmatrix} 1 \\ 0 \end{pmatrix} + \frac{\hbar\omega}{c} \begin{pmatrix} -1 \\ 0 \end{pmatrix} &= \gamma' m_e v' \begin{pmatrix} \cos\theta_e \\ \sin\theta_e \end{pmatrix} \\ &\quad + \frac{\hbar\omega'}{c} \begin{pmatrix} \cos\theta_\gamma \\ \sin\theta_\gamma \end{pmatrix}. \end{aligned} \quad (13)$$

The left hand side of Eq. (13) contains the energies and momenta before scattering, while the right hand side shows those after. From this system of three equations, one can derive an exact expression for the scattered photon energy E'_γ:

$$E'_\gamma = \frac{E_\gamma(1+\beta)}{1 - \beta\cos\theta_\gamma + \frac{E_\gamma}{E_e}(1+\cos\theta_\gamma)}. \quad (14)$$

The maximum of E'_γ is obtained when the photon fully backscatters, i.e., $\cos\theta_\gamma \approx 1$. In the ultrarelativistic limit

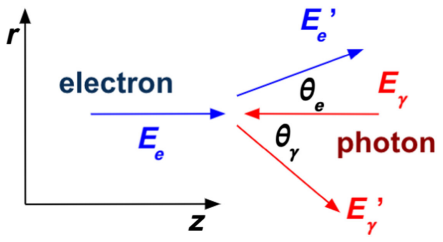

FIG. 3. Inverse Compton scattering of a photon and an electron. The scattering angle of the photon is given by θ_γ, and that of the electron by θ_e.

($\gamma \gg 1$) using the expansion $\beta \approx 1 - 1/(2\gamma^2)$ in the denominator, it can be expressed as

$$E'_{\gamma,\max} = \frac{2E_\gamma}{\frac{1}{2}\left(\frac{m_e c^2}{E_e}\right)^2 + 2\frac{E_\gamma}{E_e}}. \quad (15)$$

1. Sampling of the scattered photon energy and scattering angles

Equations (14) and (15) with different conventions of the scattering angles and coordinate system can also be found in [22]. Using the assumption that the energy of the virtual photons is negligible compared to the beam energy, i.e., $E_\gamma \ll E_e$, the scattered photon energy from Eq. (14) can be expressed as a fraction of the maximum energy $E'_{\gamma,\max}$ [23]:

$$E'_\gamma = \frac{E'_{\gamma,\max}}{1 + \left(\frac{E_e\theta_\gamma}{E_{\rm cm}}\right)^2}, \quad (16)$$

where

$$\begin{aligned} E_{\rm cm} &= \sqrt{\left(\frac{E_e}{c} + \frac{E_\gamma}{c}\right)^2 c^2 - (p_e + p_\gamma)^2 c^2} \\ &= m_e c^2 \sqrt{\frac{4E_e E_\gamma}{(m_e c^2)^2} + 1} \approx \sqrt{4E_e E_\gamma} \end{aligned} \quad (17)$$

is the center of mass energy of the electron-virtual photon system in a head-on collision and in the ultrarelativistic limit [24]. Equation (16) tells the energy of the Compton scattered photon in terms of the scattering angle θ_γ and some kinematic variables. However, in the Monte Carlo event generation, we sample the scattered photon energy E'_γ and what we do not know initially is the scattering angle of the photon (θ_γ) and the electron (θ_e). The Compton scattering of an unpolarized virtual photon with total energy E_γ on a primary electron or positron with total energy E_e is described by the differential cross section of the backscattered photon energy [13]:

$$\sigma_{C,\rm diff}(y) = \frac{2\pi r_e^2}{s}\left[\frac{1}{1-y} + 1 - y - \frac{4y}{s(1-y)} + \frac{4y^2}{s^2(1-y)^2}\right]. \quad (18)$$

Here

$$y = \frac{\hbar\omega'}{E_e} = \frac{E'_\gamma}{E_e} \quad (19)$$

is the energy of the backscattered (real) photon in units of the total energy of the opposing primary before scattering. The parameter $r_e = 2.818 \times 10^{-15}$ m is the classical electron radius. Furthermore,

$$s \approx \frac{4E_\gamma E_e}{m_e^2 c^4} = 4\gamma^2 x \tag{20}$$

is the Mandelstam variable (center of mass energy squared) of the $e^{\pm}$-virtual photon system in the ultrarelativistic limit, normalized in units of the electron rest mass [25]. Note that here we assume a negligible collision angle (head-on collision) between the two particles. The total Compton cross section, for a given s, can be obtained by integrating Eq. (18) from 0 to $y_{\max}$:

$$\sigma_{C,\mathrm{tot}} = \int_0^{y_{\max}} \sigma_{C,\mathrm{diff}}(y)dy = \frac{2\pi r_e^2}{s}\left[\ln(s+1)\left(1-\frac{4}{s}-\frac{8}{s^2}\right) + \frac{1}{2}+\frac{8}{s}-\frac{1}{2(s+1)^2}\right], \tag{21}$$

where

$$y_{\max} = \frac{E'_{\gamma,\max}}{E_e} = \frac{s}{s+1}, \tag{22}$$

from Eq. (15), is the kinematically allowed maximum energy of the Compton scattered photon in units of the primary electron energy before collision. The integrated Compton cross section, given by [17]

$$\sigma_C(y) = \int \sigma_{C,\mathrm{diff}}(y)dy = \frac{2\pi r_e^2}{s}\left[-\ln(1-y)\left(1-\frac{4}{s}-\frac{8}{s^2}\right) + y - \frac{y^2}{2}+\frac{4y}{s}+\frac{4y}{s^2}+\frac{4}{s^2(1-y)}\right], \tag{23}$$

is hard to invert analytically, but it can be sampled by using the Newton-Raphson method. In this, first the interval boundaries $\sigma_C(0)$ and $\sigma_C(y_{\max})$ are computed for a given s. Then a random uniform sample r is drawn within this interval. Then the root of the equation

$$y = \sigma_C^{-1}(r) \tag{24}$$

is found iteratively, starting with an initial guess for y. From Eq. (16), one can express the scattering angle of the photon, measured from the direction of motion of the incoming electron:

$$\theta_\gamma = \frac{E_{\mathrm{cm}}}{E_e}\sqrt{\frac{E'_{\gamma,\max}}{E'_\gamma}-1}. \tag{25}$$

2. Computation of scattered momenta

After sampling the scattered photon energy E'_γ from Eq. (18), one can use the energy conservation law to calculate the scattered electron energy:

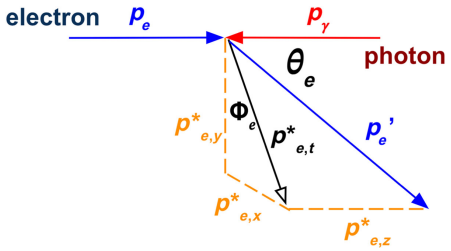

FIG. 4. Scattering of the electron in the inverse Compton scattering. The initial electron momentum p_e becomes p'_e with a transverse deviation $p^*_{e,t}$ with respect to its initial direction of motion.

$$E'_e = E_e + E_\gamma - E'_\gamma \approx E_e - E'_\gamma. \tag{26}$$

Here, we can neglect E_γ as it is typically much smaller than the other two terms. The scattered electron will be assigned a random uniform azimuthal direction, characterized by the azimuthal angle Φ_e. The kinematic momentum components will gain an extra term $p'^*_{e,i}$ due to this azimuthal deviation from the initial axis of motion. A sketch of the electron's motion after Compton scattering is shown in Fig. 4.

In addition to a change in the direction, the magnitude of the momentum components will also change because of the change in the total energy. In the ultrarelativistic limit ($|\mathbf{v}| = |\mathbf{v}'| \approx c$), we have

$$\begin{aligned}
p^*_{e,t} &= |\mathbf{p}'_\mathbf{e}|\sin\theta_e \approx |\mathbf{p}'_\mathbf{e}|\theta_e = \frac{E'_e}{m_e c^2} m_e |\mathbf{v}'|\theta_e \approx \frac{E'_e}{c}\theta_e,\\
p'_{e,x} &= p_{e,x}\frac{E'_e}{E_e} + p^*_{e,x} = \frac{E'_e}{c^2}v_x + p^*_{e,t}\sin\Phi_e,\\
p'_{e,y} &= p_{e,y}\frac{E'_e}{E_e} + p^*_{e,y} = \frac{E'_e}{c^2}v_y + p^*_{e,t}\cos\Phi_e,\\
p'_{e,z} &= \frac{\sqrt{E'^2_e - p'^2_{e,x}c^2 - p'^2_{e,y}c^2 - (m_e c^2)^2}}{c^2}.
\end{aligned} \tag{27}$$

Finally, the scattered photon momenta can simply be obtained from momentum conservation:

$$p'_{\gamma,i} = p_{e,i} + p_{\gamma,i} - p'_{e,i}, \quad i \in \{x,y,z\}. \tag{28}$$

The relationship between the scattering angles of the colliding particles can be derived from Eq. (13):

$$\theta_e = -\frac{E'_\gamma}{E'_e}\theta_\gamma = -\frac{E'_\gamma}{E_e - E'_\gamma + E_\gamma}\theta_\gamma \approx -\frac{E'_\gamma}{E_e - E'_\gamma}\theta_\gamma. \tag{29}$$

Here the minus sign reflects the momentum conservation, namely that the two particles scatter in the opposite transverse direction, as shown in Fig. 3. This derivation holds only in the ultrarelativistic limit, in case the virtual photon energy E_γ is negligible compared to the primary energy E_e (i.e., soft photon scattering) and the virtual

photons and the opposite primary collide head-on (paraxial approximation) [26].

III. EVENT GENERATION OF RADIATIVE BHABHA PHOTONS IN XSUITE

The event generation described in the previous sections is used in GUINEA-PIG [27], which is a particle in cell (PIC) solver designed to simulate a single beam-beam collision and various physical processes contributing to detector background events. For our implementation, we adopted parts of this algorithm, however, the implementation required some optimization due to the soft-Gaussian approximation used in XSUITE, which enables to be fast enough for multiturn tracking with a large number of macroparticles. The modeling of beam-beam interactions in XSUITE, taking into account collisions with a crossing angle, is detailed in [28,29]. Our model for radiative Bhabha scattering event generation is effective in the sense that the XSUITE beam-beam model does not use a PIC solver, i.e., the bunches are sliced longitudinally but not transversally. Instead, the transverse distribution is modeled in the soft-Gaussian approximation [30], by assuming a 2D Gaussian charge distribution, which is in most cases a good approximation for lepton beams.

In the following, we will consider the collision of a single pair of bunches and refer to them as weak and strong bunch, respectively. Let us consider a slice of the strong bunch, with an average energy E_c, centered at the transverse coordinates (x_c, y_c). The normalized charge density of the slice in the soft-Gaussian approach can be written as

$$\rho_e(x,y) = \frac{1}{2\pi\sigma_x\sigma_y}\exp\left(-\frac{(x-x_c)^2}{2\sigma_x^2}-\frac{(y-y_c)^2}{2\sigma_y^2}\right). \quad (30)$$

A single macroparticle from the weak bunch having the transverse coordinates (x, y) at the collision point with the slice will interact with an $N_e(x, y)$ amount of real charges, contained in an infinitesimal area $\delta x\delta y$ around (x, y):

$$N_e(x,y) = N_{b,s}\rho_e(x,y)\delta x\delta y, \quad (31)$$

where $N_{b,s}$ indicates the total number of charges in the opposing slice. A sketch of the simulation model is shown in Fig. 5.

In our model, the macroparticles of the opposing slice are replaced by a set of equivalent photons by assuming that the virtual photon distribution $\rho_\gamma(x, y)$ is proportional to that of the primary charges, i.e., $\rho_\gamma(x, y) = n_{\text{tot}}\rho_e(x, y)$. This in turn implies the following relation for the number of equivalent photons N_γ in the area $\delta x\delta y$:

$$N_\gamma(x,y) = n_{\text{tot}}N_e(x,y), \quad (32)$$

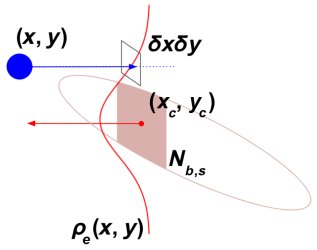

FIG. 5. Interaction of a single macroparticle of the weak bunch (blue) with a single slice of the opposing strong bunch with centroid coordinates (x_c, y_c), and total elementary charge $N_{b,s}$ (red), at the transverse coordinates (x, y). The charge density of the bunch slice is approximated with a 2D Gaussian $\rho_e(x, y)$, given in Eq. (30).

with n_{tot} from Eq. (9) representing the number of virtual photons equivalent to one elementary charge.

The event generation process of XSUITE consists of a loop over the macroparticles in one slice of one bunch, which interacts with one slice of the opposing bunch. For each macroparticle, the algorithm first computes $\rho_e(x, y)$ according to Eq. (30) by using the rms sizes of the opposing bunch slice. Next, the full slice of the opposing bunch is treated as a single macroparticle with energy E_c and n_{tot} equivalent photons are drawn for this energy, using Eq. (9). The virtual photon energies E_γ and virtualities Q^2 are sampled from the virtual photon distribution in Eq. (3). The beam size effect can be taken into account by smearing the transverse coordinates of each virtual photon with respect to the slice centroid (x_c, y_c), using the impact parameter according to Eq. (12). The charge density ρ_e is then resampled at the new transverse coordinates.

In a nested loop over the virtual photons interacting with the single macroparticle, the number of inverse Compton scattering events R for each macroparticle-virtual photon pair is computed

$$R = \sigma_{C,\text{tot}}L_{m,s}, \quad (33)$$

using the total Compton cross section $\sigma_{C,\text{tot}}$ [Eq. (21)] and the luminosity $L_{m,s}$. This luminosity corresponds to an integrated value over the passage of the single macroparticle through the single slice, with the collision of $N_e(x, y)$ charges from the opposing slice and $N_{b,m}$ charges represented by the macroparticle. It can be given as

$$L_{m,s} = \frac{N_{b,m}\times N_e(x,y)}{\delta x\delta y} = N_{b,m}N_{b,s}\rho_e(x,y), \quad (34)$$

where we used Eq. (31) to express the charge represented by the slice in terms of the charge density at the coordinates (x, y). The total Compton cross section expresses the probability of a Compton scattering event in the electron-virtual photon system: $\sigma_{C,\text{tot}} = \sigma_{C,\text{tot}}(s)$, dependent on s, given by Eq. (20). Substituting these into Eq. (33), one

obtains the number of inverse Compton scattered photons (i.e., the emitted radiative Bhabha photons) coming from the collision of the single macroparticle with one virtual photon of the opposing slice

$$R = \sigma_{C,\mathrm{tot}}(s) N_{b,m} N_{b,s} \rho_e(x,y). \tag{35}$$

Note that R can be larger than 1 due to the luminosity scaling, since the virtual photons are related to the total number of primary charges in the opposing slice. In simulations, R is rounded up to the nearest integer. Its typical value depends on $L_{m,s}$, therefore, on the number of macroparticles and the number of slices in the opposing bunch, for a given simulation setup. For the FCC-ee, a typical simulation features 100 slices and 10^6 macroparticles, for which R is close to 0, therefore, only 1 Compton event per electron-virtual photon pair is simulated, for all operation modes. If instead we only take 1 macroparticle, which represents the full intensity of the weak bunch, and 100 slices, R has values up to the order of 10^4 for the $\mathrm{t\bar{t}}$ and order of 10^5 for the Z operation mode, which is explained mainly due to the smaller transverse spot size for the Z mode which results in roughly one order of magnitude larger values for $\rho_e(x,y)$ for Z than $\mathrm{t\bar{t}}$. In comparison, the dependence of R on $\sigma_{C,\mathrm{tot}}$, thus the beam and the sampled virtual photon energy, is negligible. For $\sigma_{C,\mathrm{tot}}$, the typical values with the FCC-ee parameters are in the order of millibarns. The value of R is larger when interacting with slices in the longitudinal center of the opposing bunch, for which $N_{b,s}$ is larger, than when interacting with slices in the longitudinal bunch tails. For each of the R Compton events, s is computed according to Eq. (20) and then the scattered photon energy y is drawn according to Eq. (18). Following this, the scattered momentum components, angles, and primary energy are computed according to the equations in Sec. II. Because of the scaling with the number of charges used in Eq. (34), R represents a number of real photons, unlike the virtual "macrophotons," which represent the equivalent field of a set of real primary charges, analogous to the macroparticles. Therefore, the dynamical variables of the macroparticles are updated according to the energy and momentum conservation accounting for the emission of only a fraction of the photons. The latter are picked randomly based on a probability corresponding to the inverse of the number of charges per macroparticle.

IV. BENCHMARK AGAINST GUINEA-PIG AND BBBREM

GUINEA-PIG is a beam-beam simulation software developed initially for linear colliders, but it is widely used across the accelerator physics community for different machines, including the FCC-ee [3]. It can simulate various background generating mechanisms, including radiative Bhabha scattering [31]. Each process requires a proper choice of the cutoff x_{min} in the virtual photon spectrum in Eq. (10). We performed a parameter scan with the two codes, which showed that the simulated radiative Bhabha cross section converges below a value of $\sim 10^{-3}/\gamma^2$. This cross section is computed as

$$\sigma_{\mathrm{Bhabha}} = \frac{R_k}{L_{\mathrm{int}}}, \tag{36}$$

with R_k being the number of emitted Bhabha photons from a beam with $E'_\gamma > kE_b$, where E_b is the nominal beam energy, and k is the nominal momentum acceptance of the given operation mode.

This way the optimal cutoff value was determined to be $x_{\mathrm{min}} = 10^{-4}/\gamma^2$. With this, the value of n_{tot} is between 2 and 3 for all FCC-ee energies.

While the main concern for Bhabha lifetime are beam particles that lose an energy higher than the momentum acceptance and are rapidly lost, there exist particles that lose a fraction of their total energy due to emitting one or more radiative Bhabha photons yet remain within or close to the momentum acceptance. The survival rate of those particles may differ depending on the detail of the model used for the losses. While a hard-edge criterion on the momentum is often used, we aim at determining whether interplays with lattice nonlinearities or other radiative processes, such as beamstrahlung or synchrotron radiation in the rest of the lattice could affect the beam lifetime.

For this reason, we compare lifetimes for the FCC-ee, using the design parameters [32] featuring four interaction points (IPs), with three different simulation setups, namely a single collision without tracking in order to verify the correctness of the event generator, linear tracking, and nonlinear tracking. The simulation parameters are collected in Table I.

Table I contains estimates for the radiative Bhabha lifetime τ_{Bhabha}. These have been obtained by numerically integrating the analytical cross section, given by

$$\frac{d\sigma_{\mathrm{Bhabha}}}{dk} = \frac{4r_e^2\alpha}{k}\left[\frac{4}{3} - \frac{4}{3}k + k^2\right] \times \left[\log(4\gamma_+\gamma_-) + \log\frac{1-k}{k} - \frac{1}{2}\right], \tag{37}$$

where k is the momentum acceptance from Table I and $\gamma_\pm$ are the relativistic Lorentz factor of the e^+ and e^- beams [9]. However, these estimates do not take into account the beam size effect. As pointed out in Sec. II, with the beam size effect included, the cross section is reduced by approximately a factor of 2, and the lifetime is approximately doubled. In this paper, we refine these estimates by obtaining τ_{Bhabha} from multiturn tracking simulations (including the beam size effect) for the first time.

TABLE I. Selected parameters of the FCC-ee 4 IP design used for the simulations in this paper. The values for L_{int} are calculated using Eq. (39). All other values are taken from [32]. The quantity $\epsilon_{y,\text{lattice}}$ denotes the equilibrium vertical emittance defined by synchrotron radiation, used for the simulations in Secs. IV and V. The quantity $\epsilon_{y,\text{BB}}$ denotes that resulting from the interplay of lattice nonlinearities and beam-beam in a full lattice model, used for the simulations in Sec. VI. The subscript SR stands for synchrotron radiation and BS for beamstrahlung.

	Z	$W^{\pm}$	ZH	$t\bar{t}$
Circumference (km)		90.658816		
ϕ (mrad)		30		
E (GeV)	45.6	80	120	182.5
N_b (10^{11})	1.51	1.45	1.15	1.55
β_x^* (m)	0.11	0.22	0.24	1
β_y^* (mm)	0.7	1	1	1.6
ϵ_x (nm)	0.71	2.17	0.71	1.59
$\epsilon_{y,\text{lattice}}$ (pm)	0.75	1.25	0.85	0.9
$\epsilon_{y,\text{BB}}$ (pm)	1.4	2.2	1.4	1.6
$\sigma_{z,\text{SR}}$ (mm)	5.6	3.47	3.4	1.81
$\sigma_{z,\text{BS}}$ (mm)	12.7	5.41	4.7	2.17
$\sigma_{\delta,\text{SR}}$ (10^{-4})	3.9	7	10.4	16
$\sigma_{\delta,\text{BS}}$ (10^{-4})	8.9	10.9	14.3	19.2
Φ (1)	21.7	3.7	5.4	0.82
Q_x (1)	218.158	218.186	398.192	398.148
Q_y (1)	222.2	222.22	398.358	398.182
Q_s (1)	0.029	0.081	0.032	0.091
k (momentum acceptance) (%)	± 1	± 1	± 1.6	$-2.8/+2.5$
$\tau_{z,\text{SR}}$ (turns)	1158	219	64	18
L_{int} (10^{28} cm^{-2})	3.04	4.24	3.92	7.34
τ_{Bhabha} (min)	22.3	16.17	14	12.17

As a first check, the lifetimes from a single collision in the XSUITE weak-strong (only one beam is tracked) and strong-strong (both beams are tracked) models were investigated. In these single collision simulations, beamstrahlung is not included, but the beams are initialized with the equilibrium bunch length $\sigma_{z,\text{BS}}$ and energy spread $\sigma_{\delta,\text{BS}}$, which are determined by beamstrahlung. The Bhabha lifetime can be estimated in the following way [33]:

$$\frac{1}{\tau_{\text{Bhabha}}} = \frac{1}{N_b}\frac{dN_b}{dt} = \frac{1}{N_b}\sigma_{\text{Bhabha}} L_{\text{inst}} \times N_{\text{IP}} = \frac{1}{N_b} R_k \times f_{\text{rev}} \times N_{\text{IP}}, \tag{38}$$

where τ_{Bhabha} is the lifetime, $\frac{dN_b}{dt}$ is the charge loss rate, N_b is the bunch intensity, σ_{Bhabha} is the radiative Bhabha cross section (corresponding to a given energy cut k), $L_{\text{inst}} = L_{\text{int}} f_{\text{rev}}$ the instantaneous luminosity per collision, L_{int} is the integrated luminosity per bunch crossing, given by

$$L_{\text{int}} = \frac{N_b^2}{4\pi\sigma_y^*\sigma_x^*\sqrt{1+\frac{\sigma_{z,\text{BS}}^2}{\sigma_x^{*2}}\tan^2(\frac{\phi}{2})}} = \frac{N_b^2}{4\pi\sigma_y^*\sigma_x^*\sqrt{1+\Phi^2}}, \tag{39}$$

with Φ being the Piwinski angle. Furthermore, N_{IP} is the number of IPs in the collider, f_{rev} is the FCC-ee revolution frequency, and R_k, from Eq. (36), is the count of emitted real Bhabha photons with a total energy above the threshold kE_b. Note that this formula does not take into account the hourglass effect, which impacts the luminosity in the simulations. We compared the luminosities obtained from simulating a single collision with XSUITE against those from GUINEA-PIG, shown in the top subfigure of Fig. 6.

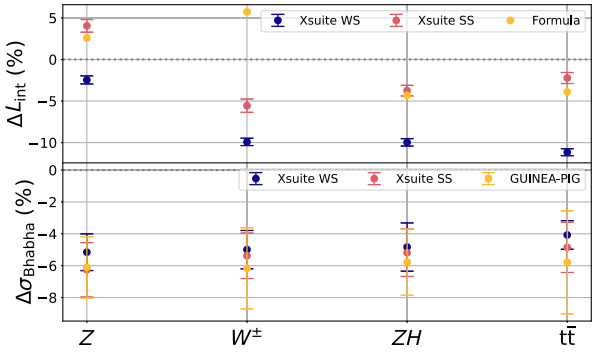

FIG. 6. Top: relative error of simulated (blue and red), as well as analytically estimated [yellow, using Eq. (39)] luminosity per bunch crossing compared to the reference values, simulated with GUINEA-PIG. Bottom: relative error of simulated Bhabha cross section compared to the reference values obtained from BBBREM. Error bars denote the statistics of repeating the simulations 20 times.

TABLE II. Radiative Bhabha scattering cross sections for the FCC-ee 4 IP design operation modes, obtained from the statistics of running BBBREM 100 times, including the beam size effect with a cutoff corresponding to the nominal rms vertical equilibrium beam size at the IP, and the nominal momentum acceptance. The statistical uncertainty is around 1% for all energies.

FCC-ee pole	Z	$W^{\pm}$	ZH	$t\bar{t}$
$\sigma_{\text{Bhabha}}^{\text{BBBREM}}$ (barn)	0.1487	0.1541	0.1341	0.1201

Here we show the relative error on the luminosity, which we estimated as

$$\Delta L_{\text{int}} = \frac{L_{\text{int}}^{\text{XSUITE}} - L_{\text{int}}^{\text{GUINEA}}}{L_{\text{int}}^{\text{GUINEA}}}. \tag{40}$$

In the weak-strong model, a large fraction of the relative error can be explained by the underestimation of luminosity by XSUITE due to the fact that the beam distribution change of the strong bunch is not modeled during the collision. In the strong-strong model, the relative errors are less than 5% for all energies, and result from the use of the soft-Gaussian approximation as opposed to the numerical solver employed in GUINEA-PIG. The relative error on the analytical expression with Eq. (39), with respect to GUINEA-PIG is explained by the absence of the hourglass effect in the formula.

The FCC-ee CDR [1] contains predictions for τ_{Bhabha}, which were estimated using cross sections obtained from BBBREM [34] (rounded to 0.15 barn for each energy) and nominal luminosity values obtained by numerical integration of the luminosity formula including hourglass effect and crossing angle. Instead of a fixed value for σ_{Bhabha}, here we have obtained the actual cross sections from BBBREM, shown in Table II.

Regarding the cross section, we benchmark values obtained both from XSUITE and GUINEA-PIG against those from BBBREM in Table II. On the bottom subfigure of Fig. 6, we show the relative error to the reference value, estimated as

$$\Delta\sigma_{\text{Bhabha}} = \frac{\sigma_{\text{Bhabha}}^{\text{XSUITE/GUINEA}} - \sigma_{\text{Bhabha}}^{\text{BBBREM}}}{\sigma_{\text{Bhabha}}^{\text{BBBREM}}}, \tag{41}$$

with the superscript denoting the code used to obtain the cross section. The plotted data are the number of emitted Bhabha photons above the corresponding momentum acceptance k, divided by the integrated luminosity of the collision. In all configurations and models, there is a systematic underestimation of the cross section, by about 5%. This systematic error could potentially be attributed to the use of the equivalent photon approximation. In comparison, BBBREM computes the matrix element for the process of Bhabha scattering with the full kinematics of a single photon emission down to zero scattering angle, including the dominant electron mass terms. We consider the agreement to the 5% level with BBBREM as a confirmation for XSUITE and this level of uncertainty as adequate for realistic beam lifetime estimates that also depend on beam and machine parameters that are generally not known to a better accuracy.

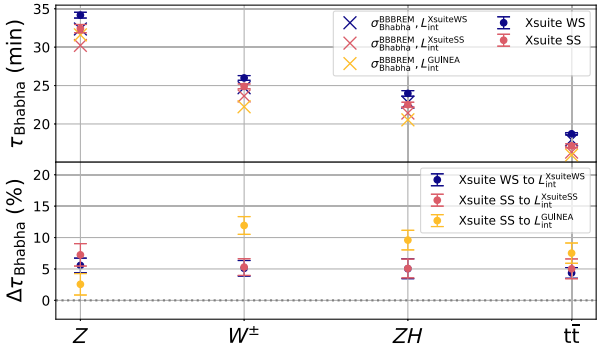

FIG. 7. Top: simulated radiative Bhabha lifetimes from the mean of 20 standalone beam-beam collisions in the XSUITE weak-strong and strong-strong models. Error bars come from the standard deviation of the 20 estimates. Different reference values are shown with crosses, all using the cross sections from Table II and integrated luminosities per bunch crossing [Eq. (39)] from different simulation sources, indicated in the legend. Bottom: relative error of the XSUITE simulated lifetimes (dots on the top subfigure) compared to the three reference values (crosses on the top subfigure).

In the following, we estimate the lifetime by performing 20 standalone single beam-beam collisions with XSUITE, using nominal equilibrium beam parameters from Table I, and making a statistical average. Beamstrahlung and the crab-waist scheme are not included in these simulations. We report the standard deviation of the averaging as the statistical uncertainty on the lifetime. Our results are shown in Fig. 7.

In Fig. 7, we report the relative error of the lifetimes, compared to the reference values, defined as

$$\Delta\tau_{\text{Bhabha}} = \frac{\tau_{\text{Bhabha}} - \tau_{\text{Bhabha}}^{\text{ref}}}{\tau_{\text{Bhabha}}^{\text{ref}}}, \tag{42}$$

where τ_{Bhabha} is the simulated lifetime calculated according to the right hand side of Eq. (38), and $\tau_{\text{Bhabha}}^{\text{ref}}$ is the reference lifetime each case calculated according to the second to last expression in Eq. (38) with the luminosity coming from the three different simulations. The simulation results agree with the reference values within 10% relative error. It can be seen that the statistical uncertainty (coming from the standard deviation of simulating the collision 20 times) does not fully explain the deviation from our reference values, which implies that there are systematic uncertainties, which can be traced back to that of the luminosity and the cross section, described earlier.

One advantage of simulating radiative Bhabha scattering with XSUITE over GUINEA-PIG is the simulation speed. In order to obtain converged values on the luminosity using GUINEA-PIG, we found that a typical simulation in the FCC-ee setting requires more than 100 grid cells in the transverse directions for higher energy, and more than 200 for low energy setups, usually chosen to be some power of 2. However, we found that with a transverse grid size of 64×64 we could already obtain converged estimates for the number of emitted Bhabha photons in case of high energy setups, such as the $t\bar{t}$. To give a specific example, we have compared the wall clock times of simulating a single collision with Bhabha scattering (and turning off the simulation of other effects) with the two codes. We used the Z (45.6 GeV) and $t\bar{t}$ (182.5 GeV) parameters from the FCC-ee CDR [1], with 10^4 macroparticles, 100 longitudinal slices, and 64 transverse grid cells in GUINEA-PIG, which can be considered as the minimum required number that produces converged photon counts. The simulation with GUINEA-PIG takes about 10 s. In comparison, the same simulation takes less than 2 seconds with XSUITE. However, increasing the number of macroparticles by a factor 10 increases the GUINEA-PIG simulation time to an order of a minute, and 10^6 macroparticles to the order of an hour. At the same time the simulation time with XSUITE stays below one minute. This difference can be attributed to the use of the soft-Gaussian approximation, which is applicable in most cases. On top of that, XSUITE is parallelized for heavier simulations, while such a parallelization is not implemented in GUINEA-PIG.

V. LIFETIME ESTIMATES FROM LINEAR TRACKING

We have performed tracking in the weak-strong model using 10^6 macroparticles in the weak beam. Our linear lattice model in XSUITE is a sequence of elements, sketched in Fig. 8.

It consists of a beam-beam element (the IP) and a linear arc element, which is a transfer matrix representing the machine arc. The arc is split into three elements and between these we insert two sextupole elements which implement the crab-waist scheme. After the beam-beam, we insert a momentum collimator element, which kills the particles if their relative energy (δ) is beyond a defined threshold. This sequence represents a superperiod of the FCC-ee ring. We track by iterating over the sequence 2×10^5 times which equals 5×10^4 turns in case of the

FIG. 8. Sequence of elements in the XSUITE linear tracking model, starting from the left end, representing one superperiod of the FCC-ee ring. Radiation is modeled in the elements represented with a yellow block.

FCC-ee 4 IP baseline operation modes. The arc segments contain an effective model for synchrotron radiation, with exponential damping and Gaussian noise excitation. The beam-beam element contains the beam-beam kick, and the generation of photons for beamstrahlung and radiative Bhabha scattering. During tracking, we record the number of alive particles as a function of the number of turns. One can estimate the lifetime due to radiative Bhabha scattering using Eq. (38) by simply counting the number of lost particles. In case there are two or more processes that result in particle loss, the loss rates can be assumed to be additive [33]. Radiative Bhabha losses typically occur at the IP, after emitting a single hard photon, which puts the primary outside of the momentum acceptance. On the other hand, losses due to beamstrahlung (and synchrotron radiation) can occur both on the momentum acceptance and on the transverse dynamic (or physical in case of the linear model) aperture. However, as it will be shown in Sec. VI, the losses due to beamstrahlung and radiative Bhabha scattering do not interplay with each other.

With these considerations, we estimate the radiative Bhabha scattering lifetime for the FCC-ee in the following way: we perform two sets of simulations using the parameters from Table I. In one set, we turn on beamstrahlung and Bhabha scattering. In the second one, we turn on only beamstrahlung. This way we can obtain the total loss rate by fitting a line on the turn by turn evolution of the bunch intensity from the first set and we similarly get the loss rate exclusively from beamstrahlung from the second. We expect that the difference of these is the loss rate coming uniquely from radiative Bhabha scattering. The lifetime can then be obtained from the inverse of the loss rate.

Figure 9 shows our results for the Bhabha scattering lifetimes with blue crosses. Using linear tracking, it could

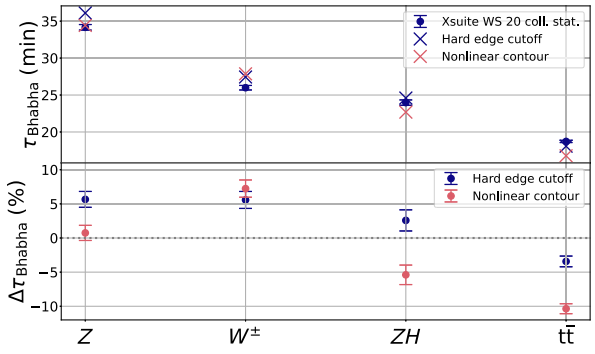

FIG. 9. Top: simulated Bhabha lifetimes from linear tracking, using a hard edge cutoff on δ (blue crosses) and the nonlinear contour extracted from the dynamic aperture (red crosses, discussed in Sec. VI). In all cases, 10^6 macroparticles were used in the weak beam, with the XSUITE weak-strong model. The reference values for both studies are the XSUITE weak-strong lifetimes from a single collision, shown in Fig. 7, shown here with blue dots. Bottom: relative error of lifetimes from linear tracking compared to the reference values. Error bars come from the statistical uncertainty of the reference value.

happen that the lifetimes are lower than the values obtained from simulating a single collision due to the interplay of the different radiation mechanisms.

We observed that the lifetimes are within 10% accuracy to those from a single collision (shown with blue dots), but not necessarily lower. The differences could be attributed to the inclusion of the crab-waist transformation at the IP in the linear tracking, which was not included in the single collision case, and which is necessary to suppress vertical blowup of the tracked bunch due to beam-beam in a multiturn tracking simulation of the FCC-ee [11]. This good accuracy is a promising sign as, like it was expected, it suggests that particle losses from radiative Bhabha scattering are not affected by other effects, such as beamstrahlung or synchrotron radiation. Here, we used the weak-strong beam-beam model, as it is approximately 2 times faster than the strong-strong one. Nevertheless, using the strong-strong model, we can expect slightly lower lifetimes (similar to the results in Fig. 7) due to the more accurate modeling of the luminosity, and a similar accuracy when compared to the single collision case using the same model.

VI. LIFETIME ESTIMATION WITH NONLINEAR TRACKING

A. Tapering

One important step that does not occur when tracking with the linear model is tapering [35]. Tapering means that the magnet strengths of all multipole elements in the lattice model have to be fine-tuned to match the energy loss caused by synchrotron radiation in the arcs. The voltage of the radiofrequency (rf) cavities in the model is consequently adjusted to compensate for this energy loss.

As a result of tapering, the closed orbit will have a varying δ along the ring. The element at which $\delta = 0$ after the tapering is referred to as the location of the tapering. From previous studies, it was found that an optimal location for tapering is at the rf insertion [36]. We found that the energy offset introduced by tapering affects the simulated lifetime as the cross section of the radiative Bhabha scattering process depends on the center of mass energy. In our simulations, the tapering location is chosen at the middle of the rf insertion for all four lattices, because this minimizes the total δ offset coming from the 4 IPs. In our nonlinear tracking study, we change the parameters of the $t\bar{t}$ mode to those from the FCC-ee midterm report, with the parameters shown in [37], since an up to date lattice model was available for this parameter set. In case of the other three operation modes, we kept the parameters shown in Table I. The δ of the closed orbit in all lattice models used in our studies, after tapering, are shown in Fig. 10.

It can be seen that the deviation from 0 increases with the beam energy. The nominal momentum acceptance has to be taken with respect to the tapered δ including this offset. The IPs, where the beam-beam elements are inserted, are marked by dots along the curves. Note that by tapering the lattice, each IP will have a different δ offset, which can affect the simulated Bhabha lifetime. Considering the magnitude of the offset, this is expected to have a negligible effect in case of all energies except for the $t\bar{t}$, where as a result of tapering the variation in the δ offset is comparable to the nominal momentum acceptance.

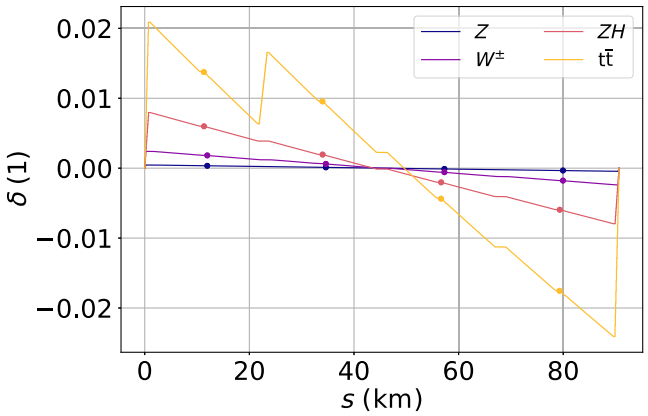

FIG. 10. Relative energy of the closed orbit after tapering at the middle of the rf insertion in case of the FCC-ee 4 IP lattices. The IPs are marked with dots. At the time of conducting these studies, the most up to date lattice for the $t\bar{t}$ mode contains two rf families [38].

B. Dynamic aperture

In Sec. V, we found that using a linear lattice with a hard edge momentum cutoff can yield a good proxy for the radiative Bhabha scattering lifetime. However, in a real lattice, particle losses are not only dependent on the momentum but also on the transverse amplitude, in a nontrivial way. Figure 11 shows the dynamic aperture of

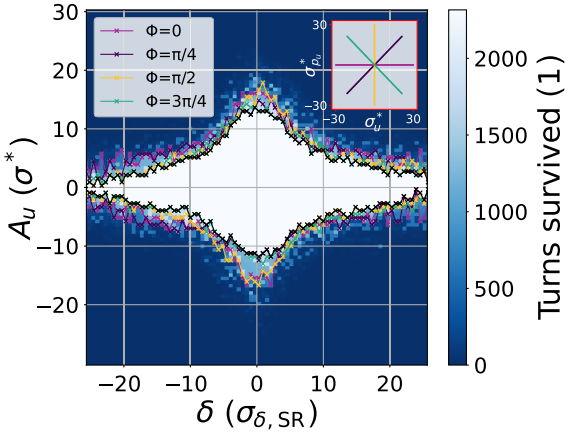

FIG. 11. Dynamic aperture of the FCC-ee Z 4 IP operation mode (using the parameters from Table I), obtained after tracking for 2500 turns with a full lattice model using mean synchrotron radiation, including beam-beam with no beamstrahlung and no Bhabha scattering. The inset plot shows the test particle grid in the transverse phase spaces.

the lattice corresponding to the FCC-ee Z 4 IP setup, obtained with XSUITE, after converting the corresponding lattice from a MAD-X format [39]. To obtain this plot, we have initialized a grid of 4×10^4 test particles at the IP, distributed in four transverse phases, with the transverse amplitudes A_u, with $u \in \{x, y\}$, defined as

$$A_u = \sqrt{\left(\frac{u}{\sigma_u^*}\right)^2 + \left(\frac{p_u}{\sigma_{p_u}^*}\right)^2} \tag{43}$$

ranging from -30 to 30 σ^* (=nominal equilibrium rms at the IP) in the transverse phase planes, as well as $\sigma_{\delta,\mathrm{SR}}$ (=nominal lattice equilibrium rms at the IP) in relative energy. For all test particles in the grid $A_x = A_y$ holds. Furthermore, all z coordinates were initialized to 0. We tracked this grid for 2500 turns (roughly the transverse synchrotron radiation damping time) and counted the number of survived turns for each particle. Each pixel on the colormap shows the number of survived turns averaged for four particles, each with a different transverse phase, but with identical relative energy δ and transverse amplitude A_u. For obtaining the dynamic aperture, the lattice was tapered at the IP, as we found that the location of tapering has a negligible effect on the dynamic aperture.

C. Location of particle losses

Although loss rates from different radiation mechanisms are additive [33], the location at which particles are lost is mostly specific to the process. To study where particles from beamstrahlung and radiative Bhabha scattering are lost, we have extracted the contour of the dynamic aperture (i.e., the borders of the white region from Fig. 11). This contour, averaged for the four phases, can be regarded as the approximate nonlinear dynamic aperture limit. We used the top right quadrant of the contour in a linear tracking model, as a refined condition for the cutoff of lost particles during linear tracking. Since tracking with a linear lattice is orders of magnitude faster than using a full nonlinear model, it is expected that this method allows to reproduce approximately the same Bhabha lifetimes while drastically reducing simulation speed. The results are shown in red in Fig. 9. In conclusion, we obtained roughly the same lifetimes as with the hard edge momentum cutoff.

More importantly, when plotting the location of macroparticle losses in the two simulation runs (beamstrahlung, Bhabha + beamstrahlung) in the $A_y - \delta$ plane as in Fig. 12, it becomes clear that particle losses due to radiative Bhabha scattering can be well separated from other particles which are lost due to simply falling out of the dynamic aperture. In the simulation where Bhabha scattering is not included, most macroparticles are lost on the vertical aperture contour. Those few particles that are located inside the vertical aperture contour are lost on the horizontal amplitude cutoff. When Bhabha scattering is turned on, some

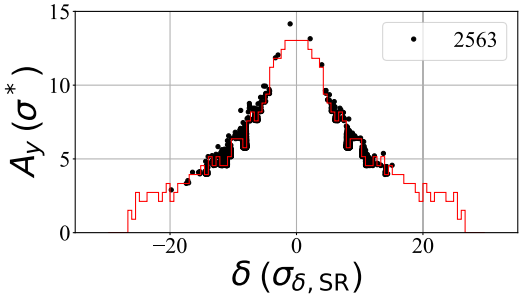

(a) With beamstrahlung only.

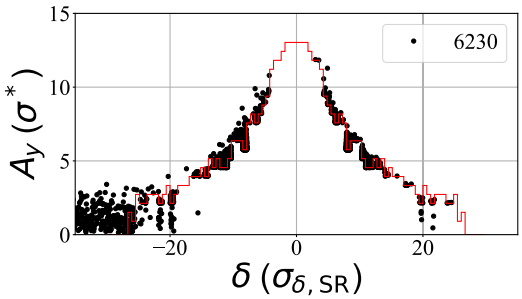

(b) With beamstrahlung and radiative Bhabha scattering.

FIG. 12. Dynamic aperture contour (top-left quadrant from Fig. 11, mirrored for the negative side) for the FCC-ee Z 4 IP lattice (using the parameters from Table I), as adopted in the linear tracking model. Lost macroparticles, after 2.5×10^4 turns, are marked with black dots at the position of loss. Simulation without (a) and with radiative Bhabha scattering (b) included. The legends show the loss count out of 10^6 initial macroparticles.

macroparticles, a comparable amount to the case with only beamstrahlung in case of the FCC-ee Z mode, are lost on the negative δ limit of the aperture. This explains why the simulated Bhabha lifetimes with this refined cutoff are similar to the case where we use the hard edge momentum acceptance. However, the extracted dynamic aperture contour is a rather strict approximation of the dynamic aperture in a real machine. Particles which lose a fraction of their energy might get beyond the momentum cutoff, but later return due to nonlinear behavior. Therefore, a verification of the lifetimes using the full nonlinear model is necessary.

D. Beam size evolution when tracking with the nonlinear lattice

With this setup, we tracked 10^5 macroparticles in the weak-strong model for 2×10^4 turns. The evolution of the rms beam sizes as well as the luminosity per bunch crossing are shown in Fig. 13. We illustrate the dynamics by showing the results for the Z and $\mathrm{t\bar{t}}$ 4 IP operation modes. Two curves are shown for each operation mode: one with and one without Bhabha scattering (BH on the plot legends) enabled. Both include quantum beamstrahlung and synchrotron radiation.

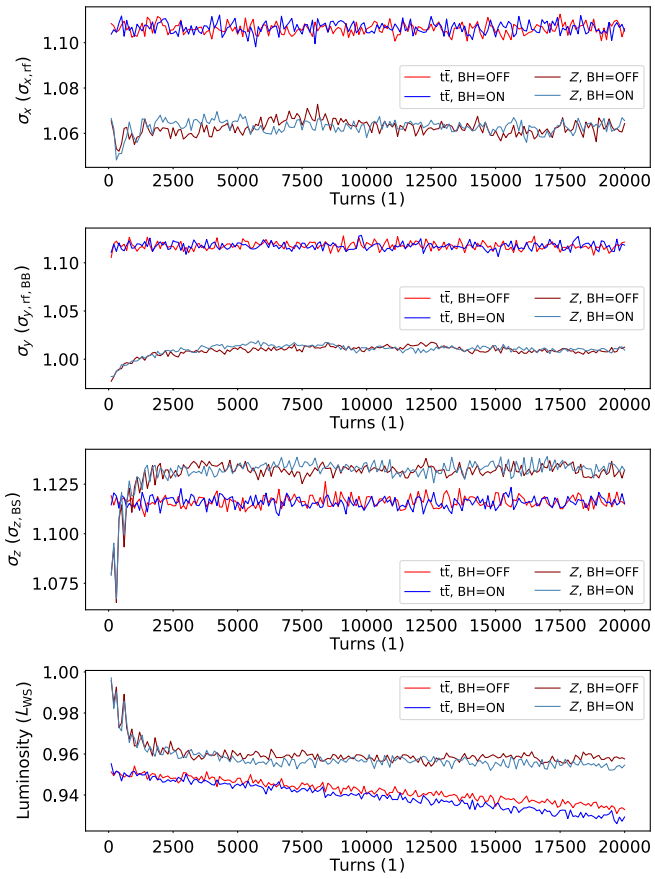

FIG. 13. Turn by turn evolution of rms beam sizes and integrated luminosity per bunch crossing of the weak bunch during nonlinear tracking. The transverse rms beam sizes are normalized to their respective value at the rf insertion, obtained from the lattice before inserting the beam-beam elements. The vertical rms normalization factor has been corrected by $\sqrt{\varepsilon_{y,\mathrm{BB}}/\varepsilon_{y,\mathrm{lattice}}}$ to account for the beam-beam blowup, with the corresponding emittances. The longitudinal rms normalization factor is the nominal bunch length including beamstrahlung. The luminosity is normalized to an estimate obtained by simulating a single collision in XSUITE in the weak-strong model.

It can be seen that Bhabha scattering has negligible effect on the beam sizes. The luminosity decreases over time due to the loss in bunch intensity. The increased number of lost particles due to radiative Bhabhas can be noticed in case of the $t\bar{t}$ resonance.

E. Lifetimes

For estimating the Bhabha lifetime, we employ the same strategy, which has been outlined in Sec. V. Figure 14 shows our results for all 4 IP operation modes. Here, the simulations have been repeated 3 times in order to obtain a statistical average on the converged lifetimes. Our reference values, obtained with Eq. (38), from the statistics of simulating 20 standalone collisions in XSUITE, are shown with dots. The interplay of beam-beam with the lattice

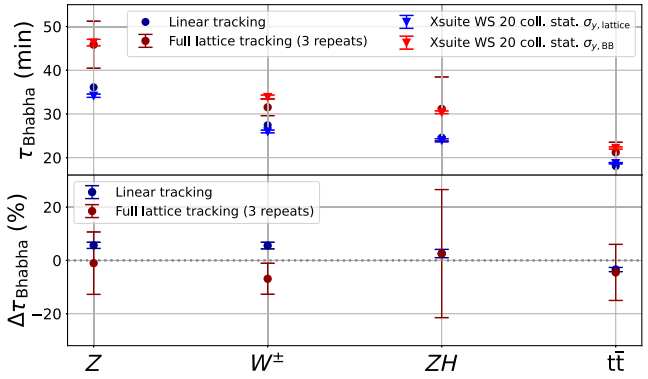

FIG. 14. Top: simulated Bhabha lifetimes from nonlinear tracking (dark red) and linear tracking from Fig. 9 (dark blue). In case of nonlinear tracking, 10^5 macroparticles were used in the weak beam, with the XSUITE weak-strong model. The triangles show our reference values, simulated with XSUITE in a setup featuring a single beam-beam pass. The blue triangles correspond the blue dots in Figs. 7 and 9. Bottom: relative error of lifetimes from linear/nonlinear tracking, compared to those from a single collision, i.e., we compare the dark red to red and dark blue to blue data points. Error bars come from the statistical uncertainty of the reference values and, in case of nonlinear tracking, from that of the three repetitions.

nonlinearities results in a blowup of the vertical rms, compared to the nominal value, by about 30%. Therefore, the reference values for nonlinear tracking are different from those shown in Fig. 7. This time, they were obtained using $\sigma_{y,\mathrm{BB}} = \sqrt{\varepsilon_{y,\mathrm{BB}}\beta_y^*}$, using the vertical emittance from Table I (from [37] for the $t\bar{t}$ case), which is the equilibrium obtained from nonlinear tracking featuring beam-beam and beamstrahlung. For comparison with our linear tracking results, the lifetimes from Fig. 9 are also plotted in Fig. 14.

In general, the simulated lifetimes are within 20% accuracy to the reference values, which can be considered a good agreement. The error could be attributed to the residual offset in δ after tapering but contributions from quantum excitation from the arc could also have an impact.

The dependence of the collision energy on the location of tapering opens the door for further studies. In a real machine, it is crucial for the experiments to collide the beams at the nominal energy. Therefore, a more sophisticated tapering strategy will be required than the one presented here. In simulations, it is likely that the two rings will have to have their own separate lattice model, which will be tapered differently. A more sophisticated tapering strategy could either include reducing the energy deviation at each IP to 0, or tuning the energy deviation such that the center of mass energy at the IPs corresponds to the nominal value.

VII. SUMMARY

In this paper, we have introduced a Monte Carlo event generator to simulate small angle radiative Bhabha

scattering, which is crucial for the beam lifetime and luminosity measurement at the FCC-ee. The algorithm is implemented in XSUITE and is optimized for multiturn tracking simulations in the soft-Gaussian approximation. We have detailed the theory and implementation of the sampling of the virtual photon and Compton scattering distributions as well as the implementation in XSUITE. We have shown that enabling Bhabha scattering in a numerical simulation featuring the full nonlinear lattice does not result in any detrimental changes in the beam profile or the luminosity. Furthermore, we have demonstrated the accuracy of the event generator on various benchmarks of the radiative Bhabha cross section and the lifetime with comparisons to the well established codes GUINEA-PIG and BBBREM, and XSUITE simulations of single collisions as well as tracking with linear and nonlinear lattice models. Moreover, we have highlighted the importance of tapering for the collision energy and in turn the lifetimes.

ACKNOWLEDGMENTS

The authors would like to thank M. Hofer, K. Oide, and L. van Riesen Haupt for help with and fruitful discussions on the setup and optimization of the nonlinear lattice models, and C. Carli for the useful comments on this paper. This work was carried out under the auspices of and with support from the Swiss Accelerator Research and Technology (CHART) program [40] and with funding from the EU Future Circular Collider Innovation Study (FCCIS) project under the Grant Agreement ID 951754 [41].

[1] M. Benedikt, A. Blondel, O. Brunner, M. Capeans Garrido, F. Cerutti, J. Gutleber, P. Janot, J. M. Jimenez, V. Mertens, A. Milanese, K. Oide, J. A. Osborne, T. Otto, Y. Papaphilippou, J. Poole, L. J. Tavian, and F. Zimmermann, FCC-ee: The Lepton Collider: Future Circular Collider Conceptual Design Report Volume 2. Future Circular Collider, CERN, Geneva, Technical Report No. CERN-ACC-2018-0057, 2019.

[2] F. Zimmermann, M. Benedikt, K. Oide, and T. Raubenheimer, The electron-positron Future Circular Collider (FCC-ee), in *Proceedings of the North American Particle Accelerator Conference, NAPAC-2022, Albuquerque, NM* (JACoW, Geneva, Switzerland, 2022), p. 315.

[3] M. Boscolo and A. Ciarma, Characterization of the beamstrahlung radiation at the future high-energy circular collider, Phys. Rev. Accel. Beams **26**, 111002 (2023).

[4] H. J. Bhabha, The scattering of positrons by electrons with exchange on Dirac's theory of the positron, Proc. R. Soc. A **154**, 195 (1936).

[5] K. Piotrzkowski, Observation of the beam-size effect at HERA, Z. Phys. C **67**, 577 (1995).

[6] J. D. Bjorken and S. D. Drell, *Relativistic Quantum Mechanics*, International Series in Pure and Applied Physics (McGraw-Hill, New York, 1964).

[7] G. Abbiendi *et al.*, Precision luminosity for Z^0 lineshape measurements with a silicon-tungsten calorimeter, Eur. Phys. J. C **14**, 373 (2000).

[8] J. Wenninger, M. Benedikt, K. Oide, and F. Zimmermann, Future Circular Collider study, Lepton collider parameters, CERN, Technical Report No. FCCACC-SPC-0003 rev. 2.0, 2016.

[9] H. Burkhardt and R. Kleiss, Beam lifetimes in LEP, Conf. Proc. C **940627**, 1353 (1995), https://accelconf.web.cern.ch/e94/PDF/EPAC1994_1353.PDF.

[10] XSUITE, https://github.com/xsuite.

[11] M. Zobov *et al.*, Crab Waist collision scheme: A novel approach for particle colliders, J. Phys. Conf. Ser. **747**, 012090 (2016).

[12] E. Fermi, Über die Theorie des Stoßes zwischen Atomen und elektrisch geladenen Teilchen, Z. Physik **29**, 315 (1924).

[13] D. Schulte, Study of electromagnetic and hadronic background in the interaction region of the TESLA collider, Ph.D. thesis, University of Hamburg, 1997, https://cds.cern.ch/record/331845?ln=en.

[14] C. F. von Weizsacker, Radiation emitted in collisions of very fast electrons, Z. Phys. **88**, 612 (1934).

[15] E. J. Williams, Correlation of certain collision problems with radiation theory, Kong. Dan. Vid. Sel. Mat. Fys. Med. **13N4**, 1 (1935), https://gymarkiv.sdu.dk/MFM/kdvs/mfm%2010-19/mfm-13-4.pdf.

[16] L. Harland–Lang, J. Jaeckel, and M. Spannowsky, A fresh look at ALP searches in fixed target experiments, Phys. Lett. B **793**, 281 (2019).

[17] V. Berestetskii, E. Lifshitz, and L. Pitaevskii, Chapter X: Interaction of electrons with photons, in *Quantum Electrodynamics*, 2nd ed., edited by V. Berestetskii, E. Lifshitz, and L. Pitaevskii (Butterworth-Heinemann, Oxford, 1982), pp. 354–455.

[18] V. M. Budnev, I. F. Ginzburg, G. V. Meledin, and V. G. Serbo, The two-photon particle production mechanism. Physical problems. Applications. Equivalent photon approximation, Phys. Rep. **15**, 181 (1975).

[19] R. Engel, A. Schiller, and V. G. Serbo, The equivalent photon approximation for coherent processes at colliders, Z. Phys. C **71**, 651 (1996).

[20] A. Blinov, A. Bondar, Y. Eidelman, V. Groshev, S. Mishnev, S. Nikitin, A. Onuchin, V. Petrov, I. Protopopov, A. Shamov, V. Sidorov, V. Tayursky, Y. Tikhonov, G. Tumaikin, A. Vorobiov, and A. Zholents, Large impact parameter cut-off in the process $e^+e^- \to e^+e^-\gamma$, Phys. Lett. B **113**, 423 (1982).

[21] G. L. Kotkin, V. G. Serbo, and A. Schiller, Processes with large impact parameters at colliding beams, Int. J. Mod. Phys. A **07**, 4707 (1992).

[22] F. Arutyunian and V. Tumanian, The Compton effect on relativistic electrons and the possibility of obtaining high energy beams, Phys. Lett. **4**, 176 (1963).

[23] I. Ginzburg, G. Kotkin, S. Panfil, V. Serbo, and V. Telnov, Colliding γe and $\gamma\gamma$ beams based on single-pass e^+e^- accelerators II. Polarization effects, monochromatization improvement, Nucl. Instrum. Methods Phys. Res. **219**, 5 (1984).

[24] C. Curatolo, I. Drebot, V. Petrillo, and L. Serafini, Analytical description of photon beam phase spaces in inverse Compton scattering sources, Phys. Rev. Accel. Beams **20**, 080701 (2017).
[25] I. F. Ginzburg, G. L. Kotkin, V. G. Serbo, and V. I. Telnov, Colliding γe and $\gamma\gamma$ beams based on the single-pass $e^{\pm}e^{-}$ colliders (VLEPP type), Nucl. Instrum. Methods Phys. Res. **205**, 47 (1983).
[26] V. Telnov, Principles of photon colliders, Nucl. Instrum. Methods Phys. Res., Sect. A **355**, 3 (1995).
[27] GUINEA-PIG, https://gitlab.cern.ch/clic-software/guinea-pig-legacy.
[28] P. Kicsiny, X. Buffat, G. Iadarola, T. Pieloni, D. Schulte, and M. Seidel, Towards beam-beam simulations for FCC-ee, in *Proceedings of the 65th ICFA Advanced Beam Dynamics Workshop on High Luminosity Circular $e^{\pm}e^{-}$ Colliders* (JACoW, Geneva, Switzerland, 2022), p. 165.
[29] P. Kicsiny, X. Buffat, G. Iadarola, T. Pieloni, D. Schulte, and M. Seidel, Benchmark and performance of beam-beam interaction models for Xsuite, in *Proceedings of the 14th International Particle Accelerator Conference, IPAC-2023, Venice, Italy* (JACoW, Geneva, Switzerland, 2023), pp. 668–671.
[30] M. Bassetti and G. A. Erskine, Closed expression for the electrical field of a two-dimensional Gaussian charge, CERN, Geneva, Technical Report No. CERN-ISR-TH-80-06, 1980.
[31] D. Schulte, Beam-beam simulations with GUINEA-PIG, eConf **C980914**, 127 (1998), https://www.slac.stanford.edu/econf/C980914/papers/F-Th24.pdf.
[32] K. Oide, FCC-ee collider optics, FCC week (2023), https://indico.cern.ch/event/1202105/contributions/5408583/attachments/2659051/4608141/FCCWeek_Optics_Oide_230606.pdf.
[33] M. Brugger, H. Burkhardt, B. Goddard, F. Cerutti, and R. G. Alia, Interactions of beams with surroundings, in *Particle Physics Reference Library: Volume 3: Accelerators and Colliders*, edited by S. Myers and H. Schopper (Springer International Publishing, Cham, 2020), pp. 183–203.
[34] R. Kleiss and H. Burkhardt, BBBREM—Monte Carlo simulation of radiative Bhabha scattering in the very forward direction, Comput. Phys. Commun. **81**, 372 (1994).
[35] L. van Riesen-Haupt, H. Burkhardt, T. H. B. Persson, and R. Tomás García, Comparison of accelerator codes for simulation of lepton colliders, in *Proceedings of the 12th International Particle Accelerator Conference, IPAC-2021, Campinas, Brazil* (JACoW, Geneva, Switzerland, 2021), p. 1334.
[36] Courtesy of K. Oide.
[37] K. Oide, Optics performance, beam lifetime, injection rate, and vibration, Future Circular Collider Innovation Study WP2 Workshop, FCCIS-2023 (2023), https://indico.cern.ch/event/1326738/contributions/5650144/attachments/2750705/4787704/Optics_Oide_231113.pdf.
[38] W. Venturini Delsolaro *et al.*, Progress and R/D challenges for FCC-ee SRF, EPJ Tech. Instrum. **10**, 6 (2023).
[39] MAD-X, https://mad.web.cern.ch/mad/.
[40] https://chart.ch
[41] https://cordis.europa.eu/project/id/951754